APPENDIX H

DEFECT DETECTION DURING MANUFACTURE OF COMPOSITE WIND TURBINE BLADE WITH EMBEDDED FIBER OPTIC DISTRIBUTED STRAIN SENSOR

Sandra M. Klute, Alex K. Sang, Dawn K. Gifford, Mark E. Froggatt
Luna Innovations Incorporated
3157 State St.
Blacksburg VA 24060

ABSTRACT

High resolution fiber optic strain sensing is used to monitor the distributed strain throughout the manufacturing process of a 9-meter wind turbine blade with intentionally introduced defects. Standard telecommunications-grade optical fiber was embedded in several layers of the carbon fiber spar cap and used to sense distributed strain during the VARTM process. The amplitude and phase of the light reflected from the fibers are measured using a commercial optical frequency domain reflectometer (OFDR). Changes in the amplitude and phase of the backscattered light were measured to determine the strain along the entire length of the spar cap with 5 millimeter resolution. Distributed strain measurements throughout the depth of the spar cap provide valuable information at intermediate points in the manufacturing process which elucidate defects both prior to and during infusion. The embedded sensors will subsequently be used to measure strain during fatigue testing of the blade to provide a cradle-to-grave method for non-destructive testing of composite structures.

1. INTRODUCTION

Current manufacturing of large Megawatt-scale wind turbine blades involves the lay-up of hundreds of individual plies of reinforcements, frequently in the form of woven or stitched fabrics, either dry or prepreg. As a result, the reinforcements are susceptible to localized in-plane waviness, out-of-plane wrinkling, delaminations, voids, and other distortions that compromise the mechanical properties of the final composite structure [1]. As the wind industry moves to scale up manufacturing processes for larger blades and the need to decrease Cost of Energy increases, it becomes imperative to detect these defects during the manufacturing process, to screen for defective parts, or ideally to correct problems in situ so that defective components can be recovered prior to final assembly.

Over the past several decades, optical fiber sensing techniques have been developed which make possible the measurement of strain profiles within a composite material. Optical fiber is ideal for this application – it is lightweight, small in diameter, immune to EMI, and composed of fused silica, which is materially compatible with most composites used in the industry. Several sensing methods have been used to provide distributed sensing over a length of fiber, including multiplexed Fiber Bragg Gratings, Brillouin scattering, and Raman scattering [2, 3]. Froggatt et. al. showed that the Rayleigh scatter signal reflected from the fiber can be used to form a fully distributed fiber sensor using a technique known as Optical Frequency Domain Reflectometry

(OFDR) [4]. The three scattering techniques make possible the use of simple, unaltered fiber as the sensor, enabling a relatively inexpensive distributed sensor. Recent work using the OFDR sensing technique has shown strain measurements with spatial resolution as fine as a few millimeters [5-7]. This high spatial resolution enables a detailed and sensitive measure of the strain profile within a composite material.

Previously, optical sensors have been embedded in composites to detect impact damage, delaminations, as well as other failures during testing [8-11]. In recent work, OFDR has been used to detect localized regions of high strain prior to the formation of a visible crack on a 9-meter CX-100 blade cycled to failure [12]. Optical fiber embedded in composite coupons has been shown to be effective in monitoring a Vacuum Assisted Resin Transfer Molding (VARTM) manufacturing process using a commercially available OFDR instrument [13]. Using this technique, the existence of resin could be detected over the length of the embedded fiber and the flow of resin through the part mapped over time. This type of monitoring is useful to detect dry areas after fabrication, where the resin has failed to wet-out the reinforcing fiber. Additionally, fiber optic sensors can be used to determine residual stresses in the component following fabrication and can remain protected within the structure to monitor strains throughout the lifetime of the component.

2. SENSING TECHNIQUE

The Rayleigh scatter amplitude reflected from an individual fiber as a function of distance is a random pattern that is formed in the fiber when the fiber is manufactured. While random, it is static and forms a unique "fingerprint" of that fiber. If a fiber is stretched, or strained, the spatial frequency of this pattern is also stretched. This elongation leads to a change in the frequency spectrum reflected from this section of the fiber. These changes can be measured and calibrated to determine the local strain in the fiber.

OFDR is an interferometric method used to measure the amplitude and phase of light reflected from an optical fiber as a function of distance [14-15]. Figure 1 shows a diagram of a basic OFDR measurement system. The light from a swept-tunable laser is split between a reference and measurement path of an interferometer using a fiber optic coupler. The light in the measurement path is sent to the fiber under test along the input port of an optical circulator. The light reflected from the fiber under test returns in the output port of the circulator. This light is then recombined with the light in the reference path. The combined signal passes through a polarization beam splitter. The polarization controller in the reference path is used control the polarization such that the reference light is split evenly between the two outputs of the polarization beam splitter. The interference pattern between the measurement and reference signals as the laser is swept across a wavelength range is recorded on two detectors, labeled S and P. A Fourier transform of these detected signals yields the amplitude and phase of the reflected light as a function of delay along the fiber. A second (trigger) interferometer with a known delay is used to compensate for nonlinearities in the laser tuning.

To find the strain at a given location in the fiber, the complex data resulting from the first Fourier transform is windowed around the desired location. The length of this window becomes the gauge length of the strain measurement. This length can be as small as a few millimeters. An inverse Fourier transform of the bandpass filtered data yields the reflected spectrum from that

section of fiber. This spectrum is cross-correlated with a spectrum from the same location measured with the fiber in a nominal, baseline state. The spectral shift between these two data sets is then converted to strain or temperature change using a calibration coefficient. This process is repeated along the fiber length to form a distributed measurement of strain along the fiber [3-6].

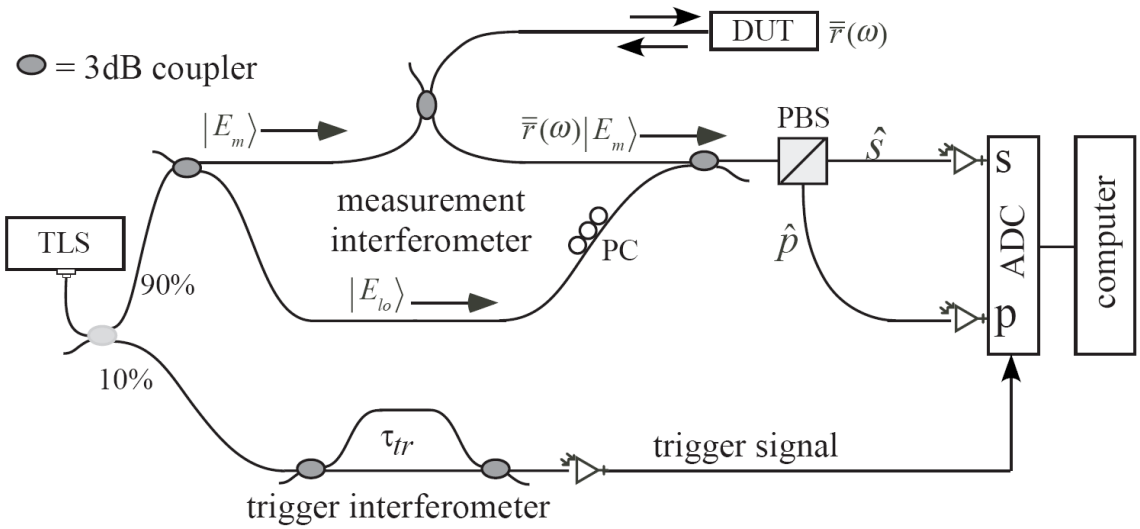

Figure 1. Basic OFDR Network

3. EXPERIMENTATION

3.1 Layup of 9-meter Wind Turbine Blade with Embedded Optical Fiber

An experimental CX-100 9-meter wind turbine blade with carbon fiber spar caps, designed by Sandia National Labs, was manufactured at TPI composites in Warren, RI. The blade was manufactured in two halves, with the High Pressure (HP) and Low Pressure (LP) sides of the blade mated after cure. Defects were cast from resin prior to lay-up and introduced into the spar cap region of the blade at three different spanwise locations, as shown in Figure 2. The three defects located from the blade root at 3.5m, 5m, and 6m had wave lengths of 45mm, 30mm, and 15mm, respectively. The wave height of all three was 3mm, for aspect ratios of 15, 10, and 5, respectively. Telecom grade, polyimide-coated, low-bend-loss fiber was used as the sensor. The polyimide coating is a commercially available rugged fiber coating that survives temperatures up to 300°C and transfers strain well to the underlying fiber. The outer diameter of the fiber with the coating is 155 micrometers. As such, it has minimal impact on the composite structure.

Optical fibers were embedded in four layers of the composite lay-up in a configuration shown in Figures 2 and 3. The fiber entered the blade along the trailing edge between stations 1000 and 2000 at the maximum chord location, progressed from the 2000 station to the 7000 station along the leading edge of the spar cap, back along the trailing edge, and exited the spar cap at the point of entry. In all layers the fiber was routed in a straight line passing through points 1” inboard of

either end of the three defects. At approximately every meter the fiber was woven into the composite material to maintain its position relative to the structure during the manufacturing process.

The first of four fibers was integrated in the +/-45 layer directly under the defects, with the second, third, and fourth fibers integrated into the triax 16, 17, and 18 layers above the defects, respectively, as shown in Figure 3. The third and fourth fibers continued on past the trailing edge data region to encompass the root of the blade. The fiber was protected with a small-diameter Teflon tubing for ingress and egress from the spar cap at the transition from carbon to balsa, where a notch of approximately 5mm was cut from the balsa to ease the fiber bend radius.

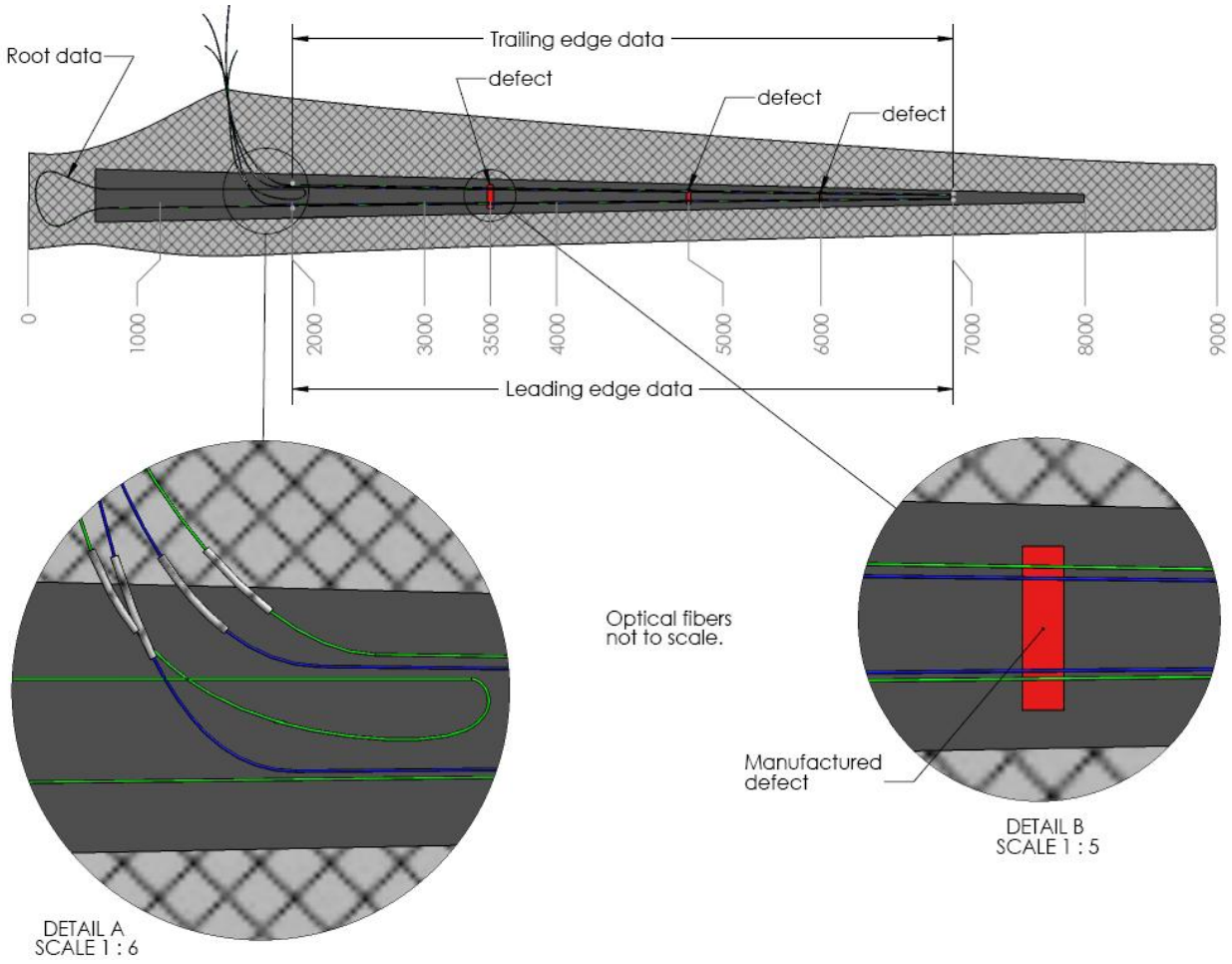

Figure 2. Drawing of High Pressure side of CX-100 blade showing optical fiber routing configuration and defect locations.

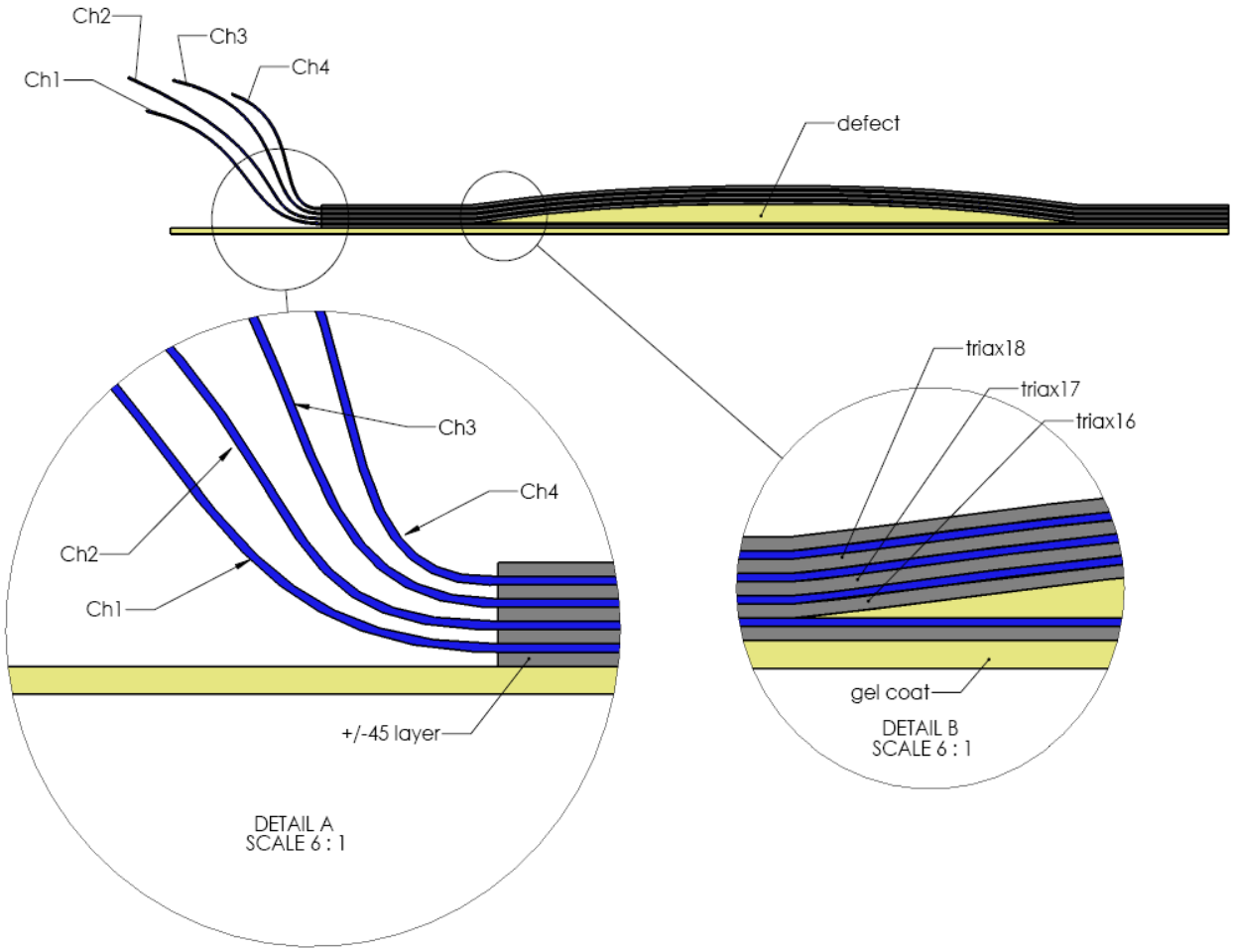

Figure 3. Sectional view of defect with optical fibers embedded in four layers of the spar cap.

3.2 Vacuum and Resin Transfer Process

The wind turbine blade was manufactured using a vacuum assisted resin transfer molding process that uses a vacuum to pull liquid resin into a dry lay-up. In the CX-100 blade the optical fiber ingress through the vacuum bag was accommodated at the trailing edge bag seam where the fibers were sealed in the seam with standard vacuum bagging tape, as seen in Figure 4. For redundancy in the sensing system, both ends of the fibers were terminated with FC/APC optical connectors so that measurements could be made from either end. The fiber egress ends were sealed in a second bag located within the primary bag in the center of the blade for later use, shown in Figure 5. Sufficient fiber was left to run these connectors out through the blade root after final assembly. The resin transfer process utilized two spiral wrap resin fill tubes, one dedicated to the root fill and the other to the fill of the remaining blade section. Both fill tubes ran along the blade spanwise at approximately the half chord location such that resin flowed quickly out towards the leading and trailing edges simultaneously.

Figure 4. Optical fiber ingress through bag seam at trailing edge for vacuum and infusion.

Figure 5. Fiber egress ends terminated with FC/APC connectors and double bagged during the infusion process.

3.2 Sensing Parameters

An Optical Backscatter Reflectometer, a commercially available OFDR system, was used to measure the reflected signal from the fiber throughout the manufacturing process. An 8-channel optical switch multiplexed the signals from the four fibers in each of the HP and LP halves of the blade. The instrument is capable of measuring up to 70 m of optical fiber with a sampling spatial resolution of up to 20 microns and strain spatial resolutions as fine as a few millimeters. For these measurements a 20 nm scan range was selected, resulting in a 40 micron sampling spatial resolution. The strain was calculated from this data with 2 and 5 mm spatial resolutions along the length of the fiber within the blade spar cap. No significant difference was seen between the data processed with the two resolutions.

4. RESULTS

4.1 Distributed Strain Measurements after Vacuum

Distributed strain data were taken throughout the manufacturing process on optical fibers embedded in both the HP and LP sides of the CX-100 blade. The measurement technique compares the state of the fiber in a reference, or baseline state, to the state of the fiber under applied strain. An initial baseline scan was taken before the sample was placed under vacuum. A vacuum was then pulled and held for a minimum of 30 minutes to ensure no leakage. Figure 6 shows strain along the leading edge region of the spar cap from the 2000 – 7000 blade station location (upper) and the trailing edge region (lower) on the HP side of the blade following the vacuum and hold. Nominal locations and widths of the defects are depicted by the rectangular elements in the lower region of each of the graphs. The defects are clearly visible in the strain data and cause peaks where the fiber is under tension relative to the small average tensile strain that exists over the entire fiber. The widths of the peaks correlate well with the widths of the defects. The double peaks are likely due to the edges of the defects creating a smaller region of higher localized strain in the fiber. Noise in the strain data was less than 5με; it is interesting to note that there is structure in the strain data along the length of the spar cap in addition to that caused by the defects.

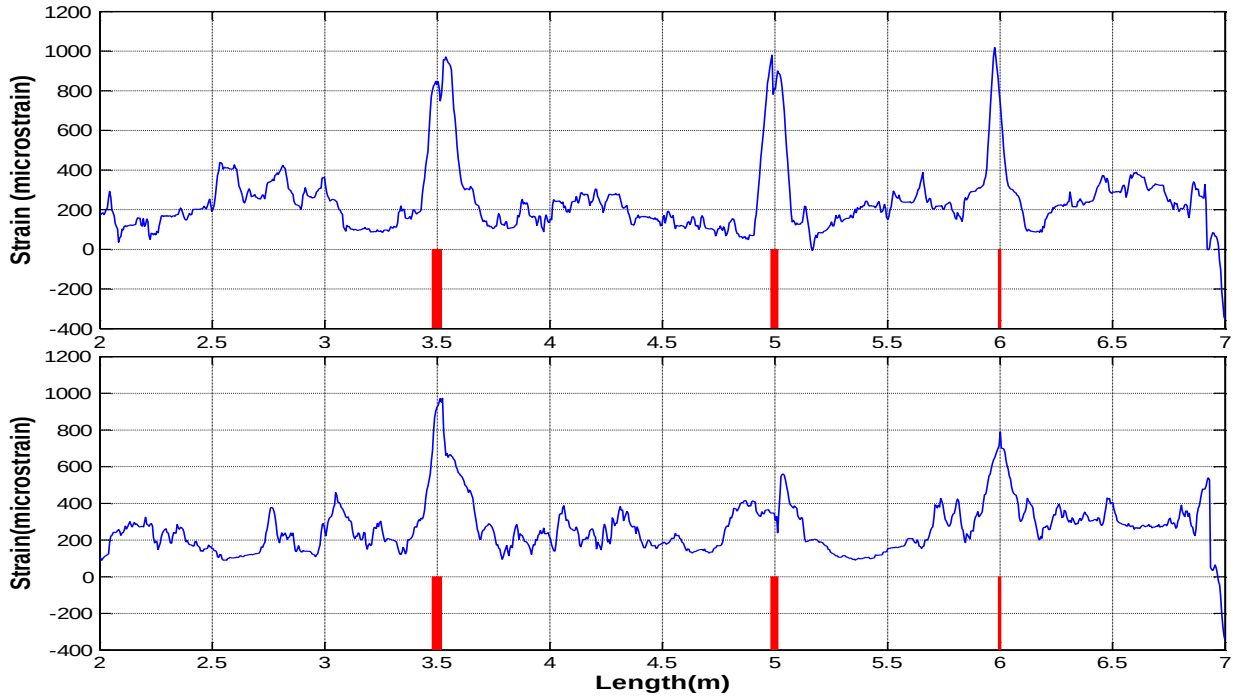

Figure 6. Distributed strain in optical fiber embedded in composite material directly under defects (ch 1) along leading edge (upper) and trailing edge (lower) of spar cap after vacuum.

Distributed strain measurements along the leading and trailing edge spar cap locations are shown in Figures 7-9 for fibers 2-4, at varying depths throughout the layup. Strain in the two triax layers directly above the defects (Figures 7 and 8) shows smaller peaks at the defect locations compared with those seen in the fiber under the defects (Figure 6).

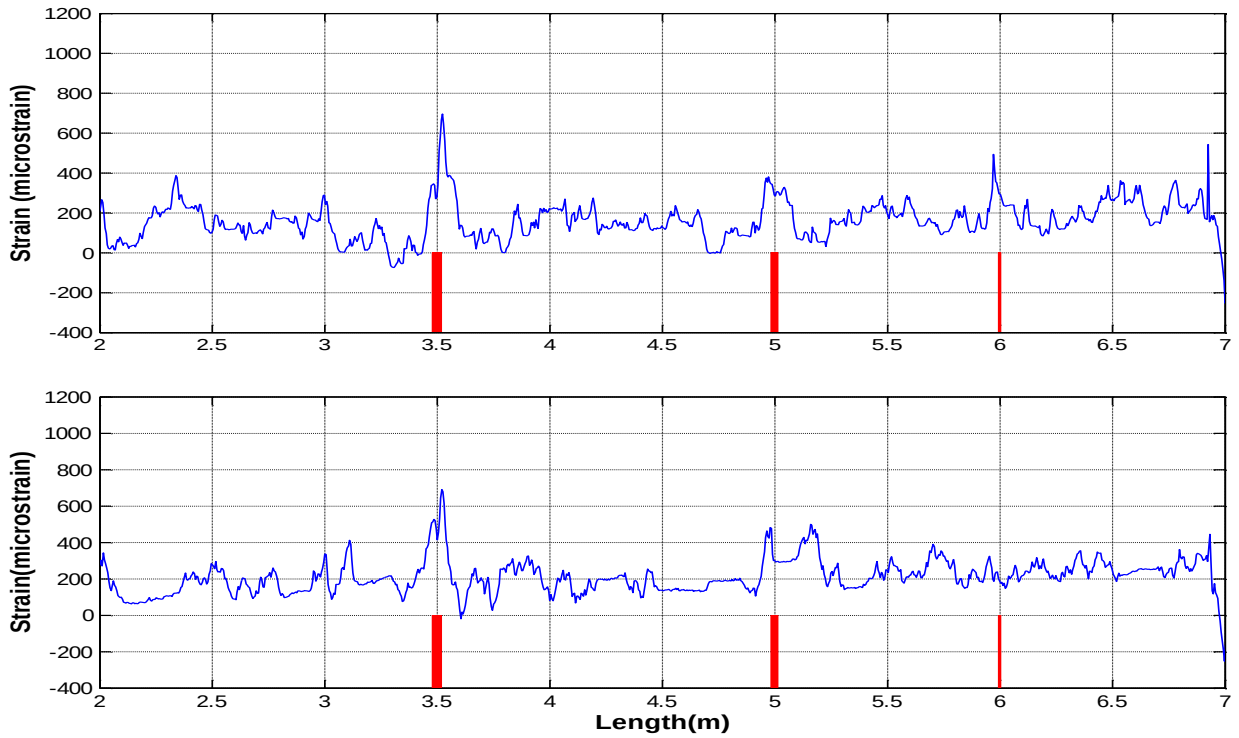

Figure 7. Distributed strain in optical fiber embedded in composite material directly above defects (ch 2) along leading edge (upper) and trailing edge (lower) of spar cap after vacuum.

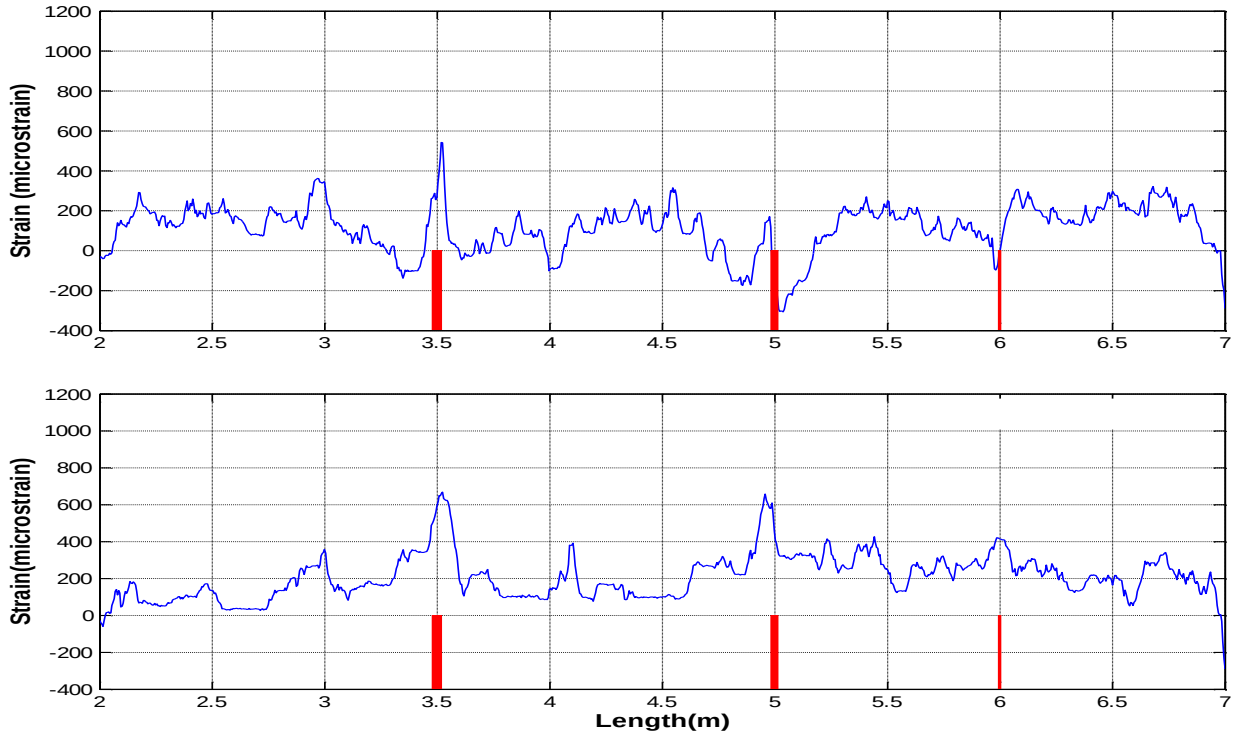

Figure 8. Distributed strain in optical fiber embedded in composite material two layers above defects (ch 3) along leading edge (upper) and trailing edge (lower) of spar cap after vacuum.

However, in the third triax layer above the defects, (Figure 9), the distributed stains are again dominated by the defects, which cause peaks where the fiber is in tension. Above the triax 18 layer blade material begins to taper in length. The strain in this fiber closest to the surface of the layup is more widely varying than in the previous layers, though with similar structure.

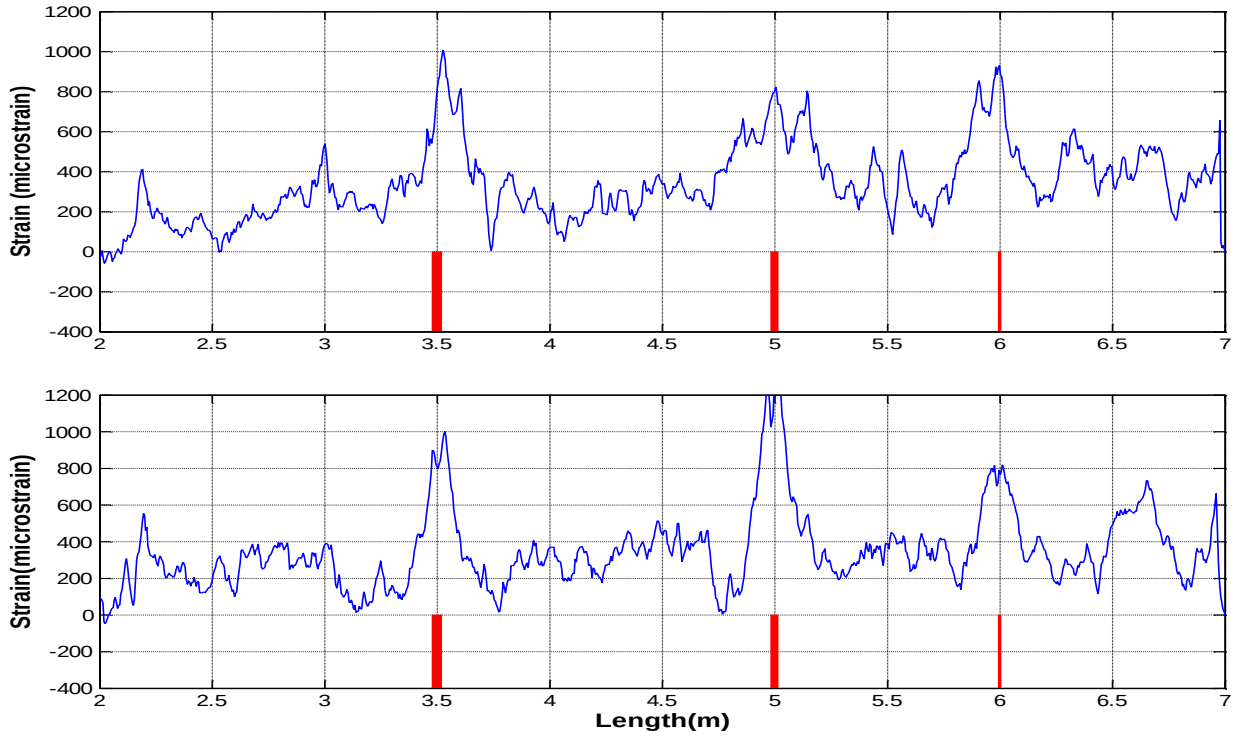

Figure 9. Distributed strain in optical fiber embedded in composite material three layers above defects (ch 4) along leading edge (upper) and trailing edge (lower) of spar cap after vacuum.

4.1 Distributed Strain Measurements During Infusion

Following the vacuum pull and hold, a new baseline measurement was taken. Strain data in the following figures are referenced to the strain state after vacuum. The infusion process was begun in the root section of the blade. Several resin feeder lines were opened, one at a time, over a period of approximately 10 minutes, beginning with a line at station 0000. In Figure 10, strain data along fiber 3 located around the root of the blade is presented for times t = (a) 0:00:00, (b) 0:01:30, (c) 0:03:00, (d) 0:05:00, (e) 0:21.30, and (f) 1:36.30 after the start of infusion. Within the first two minutes an area of higher strain can be seen around the location of the first open feeder line. The strain in this region gets larger as the resin flows and reaches a maximum of approximately 1000με at t = 5 min after the first valve was opened. In graph (e) the resin flow has reached further around the root to encompass a larger portion of the fiber, as evidenced by the larger area of significant strain, and the maximum strain caused by the flowing resin has diminished. In graph (f) the entire root fiber has been covered and the strain is more distributed.

Figure 11 presents root strain at times t = (a) t=2:01:00, (b) t=2:24:00, (c) t=2:49:00, (d) t=3:14:00, (e) t=3:39.00, and (f) t=4:04.00 after start of infusion. The exotherm process in the root causes measureable thermal strain which could be used to determine temperature and cure.

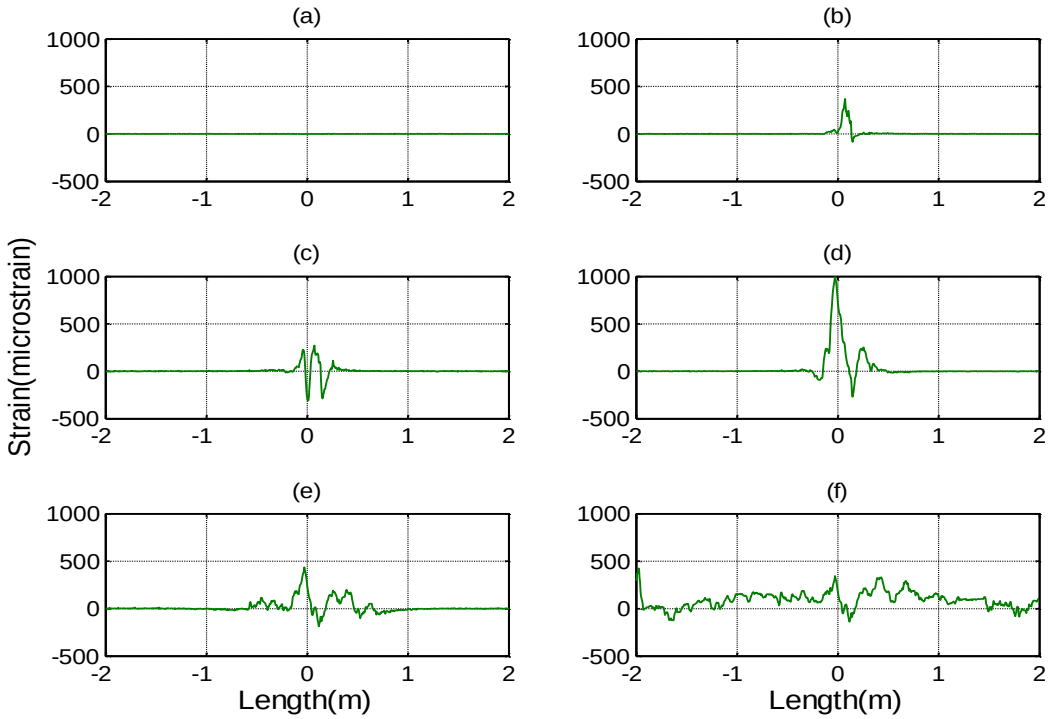

Figure 10. High Pressure blade root data at times (a) t=0:00:00, (b) t=0:01:30, (c) t=0:03:00, (d) t=0:05:00, (e) t=0:21.30, and (f) t=1:36.30 after start of infusion.

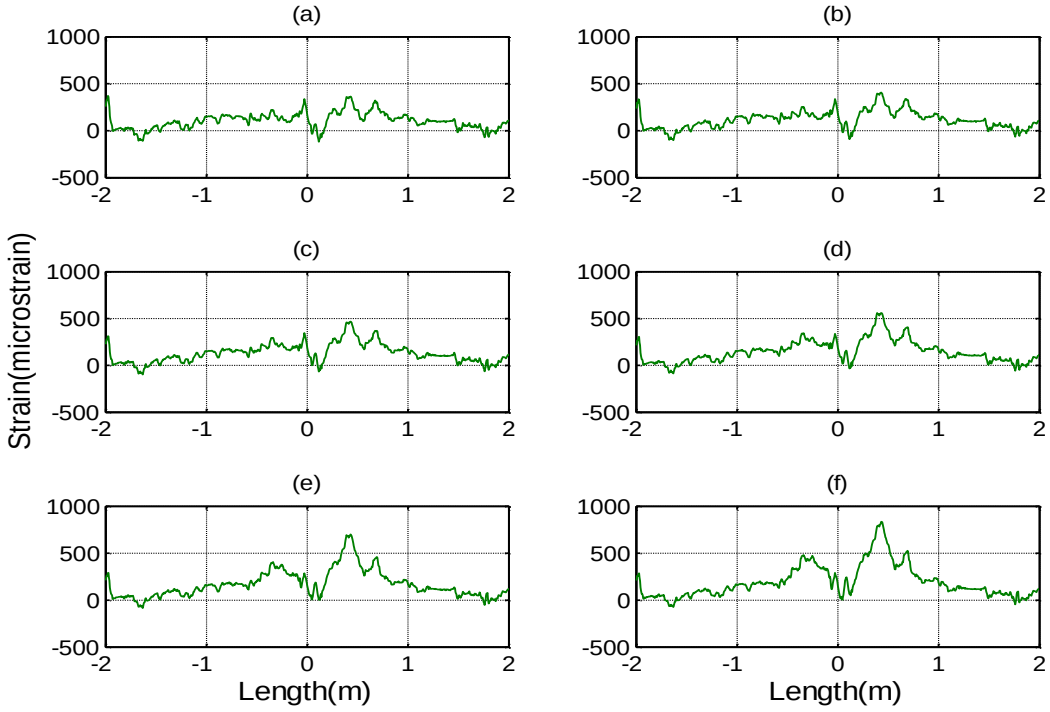

Figure 11. High Pressure blade root data at times (a) t=2:01:00, (b) t=2:24:00, (c) t=2:49:00, (d) t=3:14:00, (e) t=3:39.00, and (f) t=4:04.00 after start of infusion.

Figure 12 shows data along the fiber located under the defects (ch 1) and along the leading edge of the spar cap for six different times during the infusion process, time t = (a) 0:20:30, (b) 0:21:30, (c) 0:22:30, (d) 0:23:30, (e) 0:24:30, and (f) 1:33:30 after the start of the infusion. Here the start of the infusion is the opening of the first root valve to be consistent with the figures above; infusion of the rest of the blade began approximately 10 minutes later.

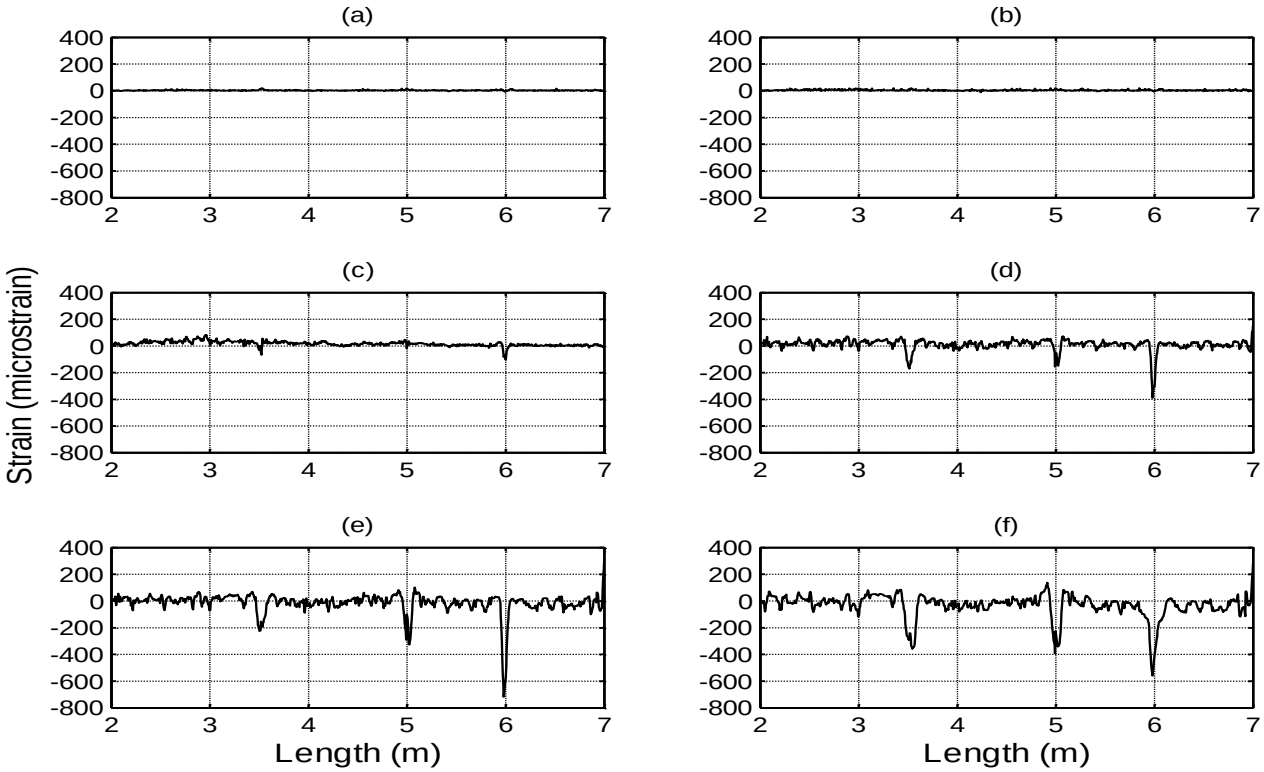

Figure 12. Distributed strain in optical fiber embedded in composite material directly under defects (ch 1) along leading edge of spar during infusion, times t = (a) 0:20:30, (b) 0:21:30, (c) 0:22:30, (d) 0:23:30, (e) 0:24:30, and (f) 1:33:30.

The defects are clear in the strain data, evidenced by compressive peaks relative to the strain state after vacuum. The vacuum appears to place the fiber surrounding the defects under tension, while the infusion relaxes that accumulated tension. The resin front, determined by regions of significant strain, moved quickly in a direction normal to the fibers such that the leading edge fiber was enveloped almost simultaneously as seen in graphs (c) and (d). As the resin continued to flow, the strains surrounding the defects decreased for the first several minutes then quickly reached steady state.

Data from fibers located in the four layers of the blade are shown in Figures 13-16 for the leading edge (upper) and trailing edge (lower) spar cap regions at times t = (a) 0:20:30 and (b) 0:21:30. The infusion can be seen to begin at t = 0:20:30 in Layers 4 and 3 of the trailing edge, and progress through Layers 2 and 1 of the trailing edge by t = 0:21:30. The spiral wrap feed line was located in close proximity to the spar cap. It appears from the strain data that it was located closer to the trailing edge; the trailing edge data shows infusion prior to the leading edge. It also appears that the resin is first introduced at a blade station of approximately 3 meters.

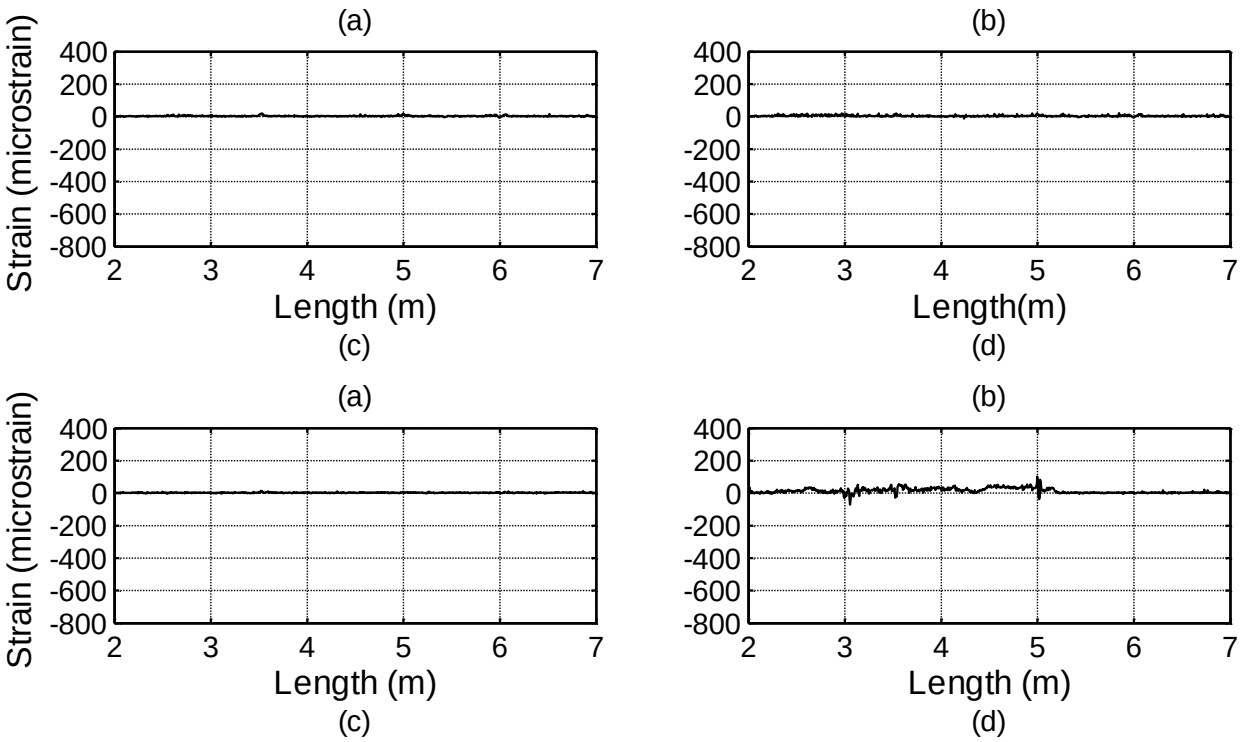

Figure 13. Distributed strain in optical fiber embedded in Layer 1 along leading edge (upper) and trailing edge (lower) of spar cap during infusion, times t = (a) 0:20:30 and (b) 0:21:30.

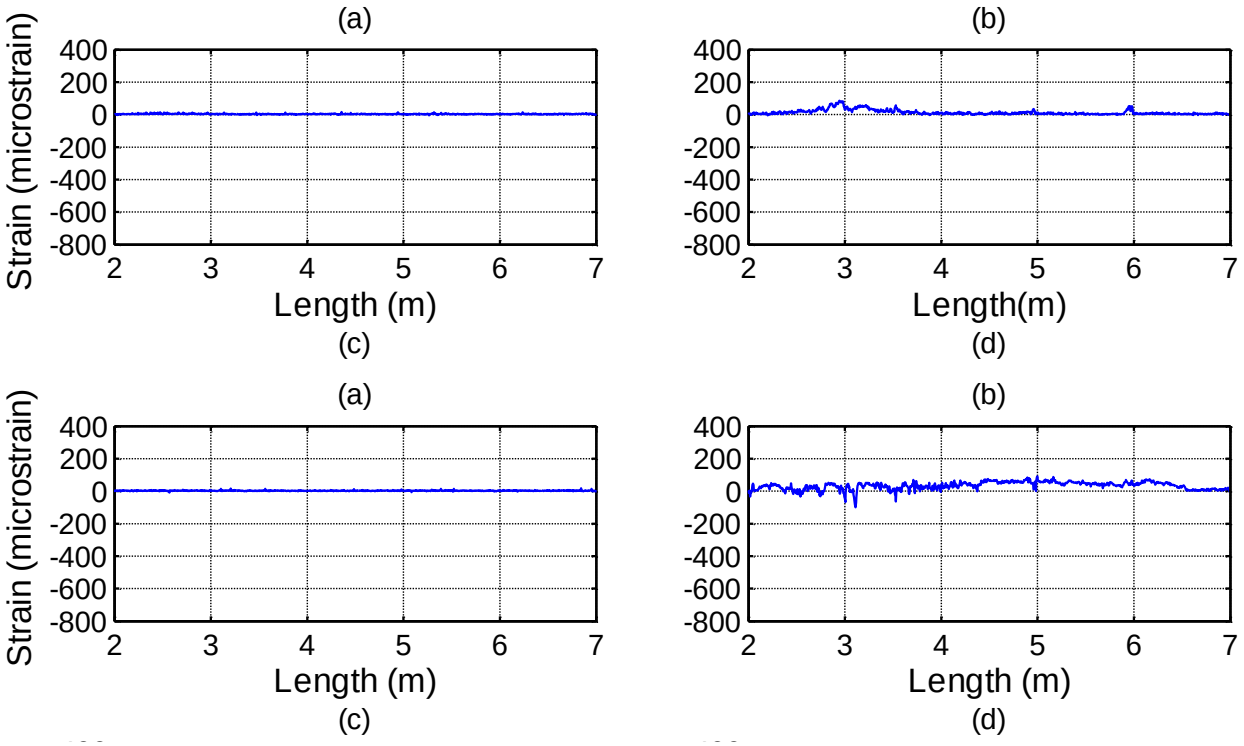

Figure 14. Distributed strain in optical fiber embedded in Layer 2 along leading edge (upper) and trailing edge (lower) of spar cap during infusion, times t = (a) 0:20:30 and (b) 0:21:30.

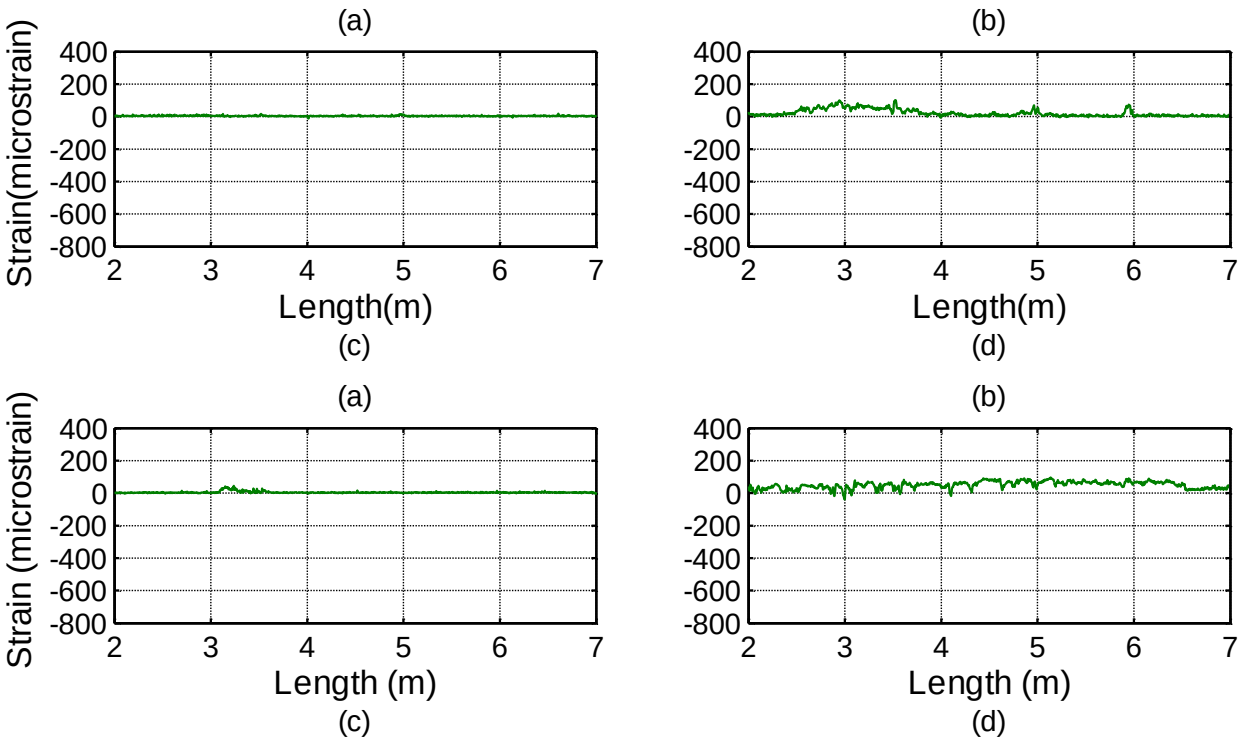

Figure 15. Distributed strain in optical fiber embedded in Layer 3 along leading edge (upper) and trailing edge (lower) of spar cap during infusion, times t = (a) 0:20:30 and (b) 0:21:30.

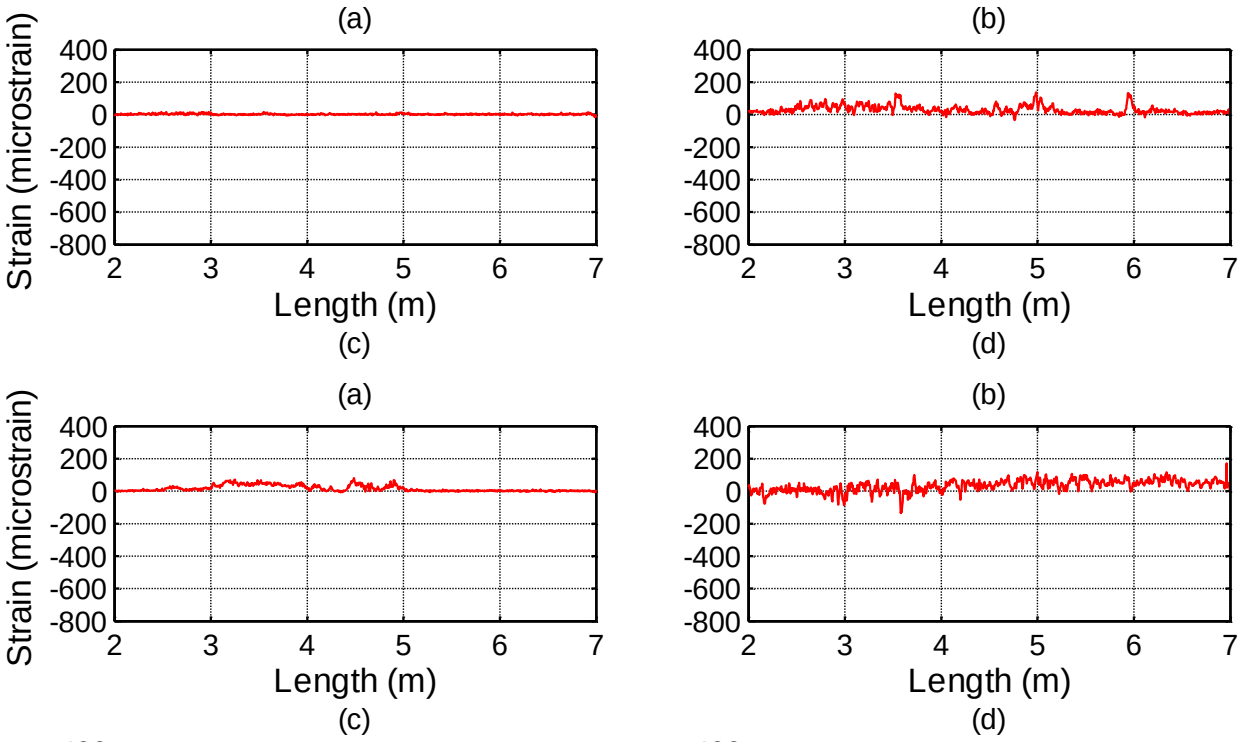

Figure 16. Distributed strain in optical fiber embedded in Layer 4 along leading edge (upper) and trailing edge (lower) of spar cap during infusion, times t = (a) 0:20:30 and (b) 0:21:30.

5. CONCLUSIONS

High resolution distributed fiber optic sensing was used to detect defects in a 9-meter wind turbine blade during a VARTM manufacturing process. Standard optical fiber was embedded in four layers of the carbon spar cap at lay-up and interrogated with an Optical Backscatter Reflectometer during vacuum and infusion. Strain data along the length of the spar cap clearly indicates locations and widths of intentionally introduced wavy defects after vacuum, both prior to and during infusion. The resin front can be seen as it propagates throughout the structure. Subsequently, thermal strains are measured during exotherm. Results provide an unprecedented view into the strain field within a composite wind turbine blade throughout its manufacturing process with millimeter scale resolution. Embedded fiber optic sensing using Optical Frequency Domain Reflectometry has the potential to provide a sensing solution throughout the life cycle of composite components.

6. ACKNOWLEDGEMENTS

Luna Innovations Incorporated wishes to gratefully acknowledge the University of Massachusetts Lowell's Wind Energy Research Group (WERG) for allowing us to participate in the Effect of Defects test, funded by the Department of Energy, as well as TPI Composites for their assistance in the blade manufacture.

7. REFERENCES

1. Berry, D. "Wind Turbine Blades Blade Mfg Improvements and Issues". *Wind Turbine Blade Reliability Workshop,* Albuquerque, New Mexico, February 24-25, 2004. http://www.sandia.gov/wind/04Presentations.htm.
2. A. J. Rogers, "Distributed optical-fibre sensing," *Meas. Sci. Technol*. 10, 75-99 (1999).
3. M. A. Davis, A. D. Kersey, "Simultaneous measurement of temperature and strain using fiber Bragg gratings and Brillouin scattering," *Proc. SPIE*, 2838, 114-123 (1996).
4. M. Froggatt and J. Moore, "High resolution strain measurement in optical fiber with Rayleigh scatter," *Appl. Opt*., 37, 1735-1740 (1998).
5. M. Froggatt, B. Soller, D. Gifford, and M. Wolfe, "Correlation and keying of Rayleigh scatter for loss and temperature sensing in parallel optical networks," *OFC Technical Digest*, paper PDP 17 (Los Angeles, March 2004).
6. B. J. Soller, D. K. Gifford, M. S. Wolfe, M. E. Froggatt, M. H. Yu, and P. F. Wysocki, "Measurement of localized heating in fiber optic components with millimeter spatial resolution," *OFC Technical Digest*, paper OFN 3, 2006.
7. S. Kreger, D. K. Gifford, M. E. Froggatt, B. J. Soller, and M. S. Wolfe, "High resolution distributed strain or temperature measurements in single- and multi-mode fiber using swept-wavelength interferometry," *OFS 18 Technical Digest*, Paper ThE42, 2006
8. R.M. Measures, Structural Monitoring with Fiber Optic Technology, 2001, San Diego, California: Academic Press
9. L. Jinsong and A. Asundi, "Structural Health Monitoring of Smart Composite Materials by using EFPI and FBG sensors, Sensors and Actuators," *A: Physical* 2003; 103(3): p. 330-340.

10. Rodrigo Silva-Muñoz and Roberto A. Lopez-Anido, "Monitoring of Marine Grade Composite Doubler Plate Joints Using Embedded Fiber Optic Strain Sensors", *Journal of Advanced Materials*, Volume 40, No. 4, October 2008, pp. 52-72
11. Guemes, A. Fernandez-Lopez, and B. Soller, Structural Health Monitoring, **9** (3), 2010, pp. 233-245
12. Kaplan, A., Klute, S. M., Heaney, A., "Distributed Optical Fiber Sensing for Wind Blade Strain Monitoring and Defect Detection." *The 8th International Workshop on Structural Health Monitoring.* Stanford, California, September 13-15, 2011. CD-ROM expected.
13. Gifford, D. K., Metry, D. R., Froggatt, M. E., Rogers, M. E., Sang, A. K., "Monitoring Strain During Composite Manufacturing Using Embedded Distributed Optical Fiber Sensing." *SAMPE Technical Conference Proceedings: 2011 - State of the Industry: Advanced Materials, Applications, and Processing Technology.* Long Beach, CA, May 23-26, 2011. Society for the Advancement of Material and Process Engineering. CD-ROM expected.
14. Brian J. Soller, Dawn K. Gifford, Matthew S.Wolfe and Mark E. Froggatt, "High resolution optical frequency domain reflectometry for characterization of components and assemblies," *Optics Express*, **13**, 2, p. 674 (2005).
15. B. J. Soller, M. Wolfe, M. E. Froggatt, "Polarization resolved measurement of Rayleigh backscatter in fiber-optic components," *OFC Technical Digest*, paper NWD3 (Los Angeles, March, 2005).